MOLECULAR IMAGING AND BIOLOGY

Mol Imaging Biol (2019) 21:25–34
DOI: 10.1007/s11307-018-1210-2

Published Online: 31 May 2018

RESEARCH ARTICLE

The Value of *In Vitro* Binding as Predictor of *In Vivo* Results: A Case for [^{18}F]FDDNP PET

Graham B. Cole,[1] Nagichettiar Satyamurthy,[1] Jie Liu,[1] Koon-Pong Wong,[1] Gary W. Small,[2] Sung-Cheng Huang,[1] Janez Košmrlj,[3] Jorge R. Barrio,[1] Andrej Petrič[3]

[1]*Department of Molecular and Medical Pharmacology, David Geffen School of Medicine at UCLA, CHS B2-086A, 694817, 10833 Le Conte Avenue, Los Angeles, CA, 90095-6948, USA*

[2]*Department of Psychiatry and Biobehavioral Sciences, Semel Institute for Neuroscience and Human Behavior, UCLA Longevity Center, David Geffen School of Medicine at the University of California, Los Angeles, CA, 90024, USA*

[3]*Faculty of Chemistry and Chemical Technology, University of Ljubljana, Večna pot 113, SI-1000, Ljubljana, Slovenia*

Abstract

Purpose: Caution is warranted when *in vitro* results of biomarkers labeled with tritium were perfunctorily used to criticize *in vivo* data and conclusions derived with the same tracers labeled with positron emitters and positron emission tomography (PET). This concept is illustrated herein with the PET utilization of [^{18}F]FDDNP, a biomarker used for *in vivo* visualization of β-amyloid and tau protein neuroaggregates in humans, later contradicted by *in vitro* data reported with [^{3}H]FDDNP. In this investigation, we analyze the multiple factors involved in the experimental design of the [^{3}H]FDDNP *in vitro* study that led to the erroneous interpretation of results.

Procedure: The present work describes full details on the synthesis, characterization, purity, and kinetics of radiolytic stability of [^{3}H]FDDNP. The optimal *in vitro* conditions for detecting tau and β-amyloid protein aggregates using macroscopic and microscopic autoradiography with both [^{18}F]FDDNP and [^{3}H]FDDNP are also presented. Macroscopic autoradiography determinations were performed with [^{3}H]FDDNP of verified purity using established methods described previously in the literature.

Results: The autoradiographic results using phosphate buffered saline (PBS) with less than 1 % EtOH and pure, freshly prepared [^{3}H]FDDNP compared with the earlier reported data using [^{3}H]FDDNP of undetermined purity and PBS in 10 % EtOH demonstrate the critical importance of rigorous experimental design for meaningful *in vitro* determinations. [^{18}F]FDDNP binding to both amyloid plaques and neurofibrillary tangles was confirmed by amyloid and tau immunohistochemical stains of adjacent tissues.

Conclusions: This work illustrates the sensitivity of *in vitro* techniques to various experimental conditions and underscores that conclusions obtained from translational *in vitro* to *in vivo* determinations must always be performed with extreme care to avoid wrong interpretations that can be perpetuated and assumed without further analysis.

Key words: [^{3}H]FDDNP, [^{18}F]FDDNP, [^{3}H]FENE, Kinetics, Autoradiolysis, Autoradiography

Introduction

In vitro binding experiments, no matter how carefully designed, are never capable of fully simulating the *in vivo* environment. The gap between a particular experimental

Electronic supplementary material The online version of this article (https://doi.org/10.1007/s11307-018-1210-2) contains supplementary material, which is available to authorized users.

Correspondence to: Jorge Barrio; *e-mail:* jbarrio@mednet.ucla.edu, Andrej Petrič; *e-mail:* andrej.petric@fkkt.uni-lj.si

design and whether that experiment can stand for a greater scientific concept—*i.e.*, *in vivo* tissue target sensitivity and specificity—is the construct validity of that experiment [1]. The key to interpreting the results of *in vitro* experiments—*i.e.*, whether or not an experiment is a valid construct—is to understand the explicit and implicit assumptions involved in the experimental design. But *in vitro* conditions are frequently designed to test a specific concept (*e.g.*, probe specificity for a tissue target) and typically ignore targets that are not designed to be tested or may not be viable under the *in vitro* experimental conditions described. For example, procedures using previously frozen brain tissue samples will inherently ignore enzymes that are inactivated due to sample handling and freezing procedures [2]. Another example is degradation of radiolabeled tracers during storage prior to use leading to erroneous conclusions. For this reason, analytical data demonstrating the purity of radiolabeled probes utilized in any investigation should always be provided. Equally important are the experimental conditions used for *in vitro* determinations which play a critical role in the assays using tissue samples. Introduction of solvents (*e.g.*, 10 % EtOH [3]) to dissolve a PET biomarker for the *in vitro* binding determinations adds an artifact that would severely affect the binding affinity of the probe to the hydrophobic aggregate sites. Moreover, for autoradiography, improper differentiation conditions [3–5] will inadequately clear background activity thereby ignoring the natural process of differentiation carried out by the body during tracer distribution *in vivo.* The conclusions drawn from the *in vitro* experimental results thus must always consider these underlying assumptions to have construct validity.

More than a decade ago, we described the experimental conditions for binding of the molecular imaging probe 1-{6-[(2-[^{18}F]fluoroethyl)(methyl)amino]-2-naphthyl}ethylidenemalononitrile ([^{18}F]FDDNP, Fig. 1) to Alzheimer's disease (AD) hallmark protein aggregates composed of senile plaques and neurofibrillary tangles [6, 7]. For digital autoradiography with [^{18}F]FDDNP, several key steps were fully described. First, [^{18}F]FDDNP purity was established, and the radiotracer was kept in 100 % EtOH to avoid any radiolytic decomposition. The radiotracer was only diluted in aqueous media immediately before use. Second, the tracer incubation was carried out in minimal EtOH (< 1 %) in PBS. Last, after primary incubation, we used either EtOH [6] or *tert*-BuOH [7] for optimal differentiation of the specific signal from the background [8]. The specific differentiation, which varies among different probes, takes the place of the natural dynamic process of tracer distribution and clearance that occurs *in vivo* resulting in specific signal of the bound tracer.

Eight years after our initial work [6, 7], Thompson et al. [3] studied the *in vitro* binding behavior of a reportedly tritiated analog of FDDNP to brain sections containing AD hallmark pathologies. Thompson et al. concluded that 2-(1-{6-[(2-fluoroethyl)(methyl) amino]-2-naphthyl} ethylidene) malononitrile (FDDNP, Fig. 1) could not efficiently detect amyloidogenic neuroaggregates, in spite of existing *in vivo* evidence obtained by [^{18}F]FDDNP with patients with multiple neurological diseases, including Alzheimer's dementia [9], progressive supranuclear palsy [10], Lewy Body dementia [11], and most recently chronic traumatic encephalopathy (CTE) [12], among others. Thompson et al. also reported that a tritiated derivative of 2-[4′-(methylamino)phenyl]-6-hydroxybenzothiazole (PIB) [13] and a C-14 labeled derivative 4-*N*-methylamino-4′-hydroxystilbene (SB-13) [14] exhibited one to two orders of magnitude higher affinity than the tritiated analog of FDDNP for amyloid plaques, under the experimental conditions described. The report of Thompson et al. [3], unfortunately, does not even disclose the chemical identity or position of the H-3/C-14 label on any of these molecules or the synthetic methods utilized for their preparations. The three tracers were simply reported as custom synthesized products without any evidence of their radiochemical purities upon receipt or at the time of the *in vitro* determinations. This is critically important considering the long known radiolytic instabilities of, especially, tritiated analogs in aqueous media [15].

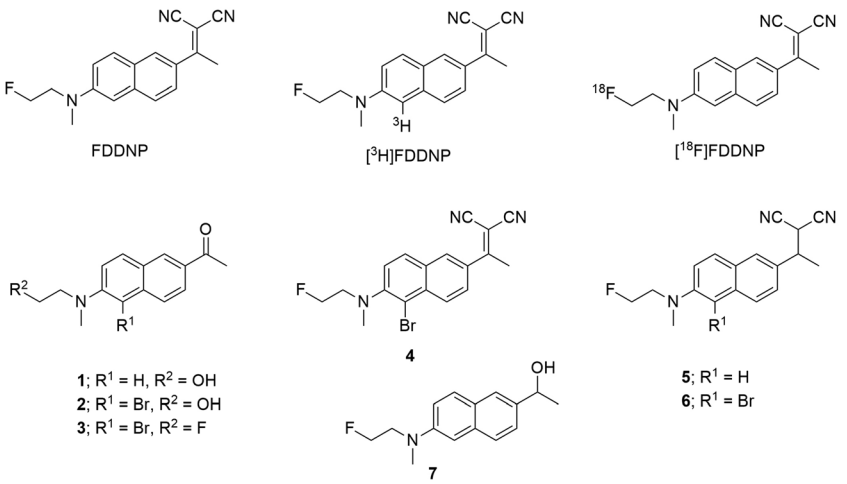

Fig. 1. Chemical structures of FDDNP, [^{3}H]FDDNP, [^{18}F]FDDNP, and of compounds **1**–**7**.

In this work, we evaluate and compare the construct validity of Thompson et al.'s conclusions [3] and extend our previous *in vitro* investigations with [^{18}F]FDDNP to include micro-autoradiography techniques. To demonstrate the identity of the key experimental reagent [^{3}H]FDDNP (Fig. 1), we have provided relevant detailed synthetic and analytical data. We have also determined the chemical and radio-stability of [^{3}H]FDDNP and conclusively demonstrated its autoradiolytic sensitivity in aqueous media under conditions generally used to perform *in vitro* binding determinations.

Materials and Methods

The description of general methods and synthetic procedures can be found in the ESM (Electronic Supplementary Material) on the journal's web page.

Tissue Handling

Postmortem brain tissue samples from subjects diagnosed with AD were obtained from the UCLA Anxiety and Depression Research Center Brain Bank (Dr. Harry Vinters, Principal Investigator). Formalin-fixed tissue samples were cryoprotected in sucrose solution beginning at 10 %, increasing to 30 % then snap frozen in 2-methylbutane in a dry ice/ethanol bath. Sections were cut at either 10 or 20 μm as indicated.

Autoradiography Procedures

The [^{3}H]FDDNP (specific activity 20.2 Ci/mmol; 1 mCi/ml in EtOH; radiochemical purity > 98 %) obtained from ViTrax as described above and the [^{18}F]FDDNP (specific activity > 3000 Ci/mmol; 1–10 mCi/ml in EtOH; radiochemical purity > 98 %) synthesized as previously reported [16] were kept in 100 % EtOH until the time of use, at which time they were diluted to < 1 % EtOH with phosphate buffered saline (PBS) unless otherwise noted.

Method of Thompson et al. [3]

Serial 20-μm sections of frontal and temporal lobe brain tissues were prepared and placed on adhesion superfrost plus slides obtained from Brain Research Laboratories (Newton, MA) and then dried prior to use. Slides were equilibrated in 10 % EtOH in phosphate buffer for 15 min prior to primary incubation with either [^{3}H]FDDNP (5 or 0.5 nM) or [^{18}F]FDDNP (2 nM) or a mixture of the two in PBS with 10 % EtOH for 60 min. Sections were washed in PBS-E twice for 30 s then once in deionized water for 30 s before being rapidly dried in air and placed on Kodak BioMAX MR film (Fisher Scientific, Pittsburgh, PA). The films were exposed for 35 min overnight to detect [^{18}F]FDDNP, and for 13, 33, or 51 weeks to detect [^{3}H]FDDNP.

Method of Agdeppa et al. [7]

Serial 20-μm sections of frontal and temporal lobe brain tissues were prepared and placed on adhesion superfrost plus slides, defatted in xylene (40 min) then rinsed in ethanol and dried prior to use. Slides were equilibrated in PBS for 15 min prior to primary incubation with either [^{3}H]FDDNP (5 nM or 0.5 nM) or [^{18}F]FDDNP (2 nM) or a mixture of the two in PBS/1 % EtOH for 25 min. Sections were then optimally washed in deionized water (30 s), 30, 40, or 50 % (*v*/*v*) *tert*-BuOH in deionized water (3 min agitated on an orbital shaker), then deionized water (30 s). Sections were dried under air and exposed to film in the same manner as described above.

Micro-autoradiography Procedures

Serial 10-μm sections of temporal lobe including the hippocampus were prepared and placed on Fisher brand superfrost slides (Fisher), and alternating slides were either defatted in xylene (40 min) then rinsed in ethanol for autoradiography or simply dried for immunohistochemistry prior to use. Slides were equilibrated in PBS for 15 min prior to primary incubation with [^{18}F]FDDNP (4 mCi/ml) in 1 % EtOH in PBS for 25 min. Sections were then optimally washed in deionized water (30 s), 30 % *tert*-BuOH in deionized water (5 min agitated on an orbital shaker), then deionized water (30 s). These conditions were optimized to provide adequate ability to resolve tau protein aggregates; however, these conditions are also adequate for resolving Aβ, though more stringent techniques will provide better images. Sections were dried under air and dipped in undiluted Hypercoat LM-1 film emulsion (GE Healthcare, Piscataway, NJ) held at 43 °C. Slides were placed at an angle and dried in ambient air to produce an even coating. Emulsion was exposed overnight and developed in Kodak D-19 developer for 1 min, stopped in 0.05 % acetic acid for 30 s, and fixed in Kodak Fixer for 5 min (Fisher).

Immunohistochemistry

Adjacent 10-μm slides to those used in the autoradiographic procedures were rehydrated in tris buffered saline (TBS). Slides in which Aβ was the target protein were treated in formic acid (FA) for 2 min and washed in TBS + 0.05 % Tween-20 (TBS-T) prior to use. All slides were blocked with 2.5 % normal horse serum for 60 min. Slides were incubated with the primary antibody for 2 h at room temperature in a humidified chamber (anti-Tau mouse monoclonal antibody, 1:50, Sigma Aldrich, St. Louis, MO; anti-Aβ mouse monoclonal, 1:50, Dako, Carpinteria, CA). Slides were washed three times for 5 min in TBS then incubated for 1 h with Vector imPRESS anti-mouse HRP labeled secondary antibody (Vector, Burlingame, CA). Slides were washed three times for 5 min in TBS then optimally incubated with 3,3′-diaminobenzidine peroxidase substrate

with metal enhancer (Sigma Aldrich). Slides were dehydrated through ethanol, cleared in xylenes, and cover slipped.

Results

Synthetic Considerations

Scheme S1 (Supplementary Material) illustrates the synthetic approach to [^{3}H]FDDNP. The synthesis begins with the electrophilic bromination of 1-(6-((2-hydroxyethyl)(methyl)amino)naphthalen-2-yl)ethanone (**1**) to yield the 1-(5-bromo-6-((2-hydroxyethyl)(methyl)amino)naphthalen-2-yl)ethanone (**2**), which upon treatment with diethylaminosulfur trifluoride (DAST) provides the key intermediate **3** (1-(5-bromo-6-((2-fluoroethyl)(methyl)amino)naphthalen-2-yl)ethanone). From the analog **3**, the synthesis of [^{3}H]FDDNP could strategically be conducted by two different methods. In the first method, a Knovenagel condensation of the bromo derivative **3** with malononitrile leads to 2-(1-(5-bromo-6-((2-fluoroethyl)(methyl)amino)naphthalen-2-yl)ethylidene)malononitrile (**4**) (Scheme S1, step *iii*). Catalytic dehalogenation of bromine in **4** with [^{3}H]H_2 gas leads to [^{3}H]FDDNP (Scheme S1, step *iv*, *Path a*). Alternatively, steps *iii* and *iv* can also be applied in reverse order to get the target compound *via* [^{3}H]FENE intermediate through *Path b*.

To identify the optimal conditions for the synthesis of [^{3}H]FDDNP outlined in Scheme S1 (Supplementary Material), the bromo analogs **3** and **4** were first prepared and independently examined as substrates in model hydrogenolysis reactions with [^{1}H]H_2. Thus, the treatment of **4** under an atmosphere of hydrogen in the presence of Pd/C for 30 min resulted in a complex mixture of products consisting of only small amounts of the desired FDDNP [16], along with two exocyclic chain hydrogenated derivatives **5** and **6**, and unreacted starting material **4** (Scheme S2, Supplementary Material). In contrast, under the same reaction conditions, the bromo derivative **3** underwent hydrogenolysis to yield 2-(1-(6-((2-fluoroethyl)(methyl)amino)naphthalen-2-yl)ethylidene)malononitrile (FENE) as the major product [16] and alcohol **7** as a minor product, along with trace amounts of unreacted **3** (Scheme S3, Supplementary Material). Based on the efficiency of the reduction process and the ease of the product purification, the reaction starting from the bromo analog **3** was deemed more appropriate for the tritium labeling method (Scheme S3, conditions *ii*).

Radiosynthesis of [^{3}H]FDDNP

[^{3}H]FDDNP was synthesized through *Path b* as outlined in Scheme S1 (Supplementary Material). The bromo compound **3** was subjected to catalytic reduction in an atmosphere of tritium gas for 30 min to provide [^{3}H]FENE in 17 % radiochemical yield. Knoevenagel reaction of the crude [^{3}H]FENE with malononitrile provided [^{3}H]FDDNP. The crude [^{3}H]FDDNP was purified by semi-preparative HPLC on a reverse phase column to yield 9.0 mCi of > 98 % radiochemically pure product with a determined specific activity of 20.2 Ci/mmol. After the evaporation of the HPLC mobile phase, the product was dissolved in absolute ethanol (1 mCi/ml) and stored at − 20 °C. Under this storage condition, the autoradiolysis of [^{3}H]FDDNP was minimized and the radiochemical purity decreased only by about 1.8 % per month.

The Radiochemical Stability of [^{3}H]FDDNP

The commercially (ViTrax) obtained [^{3}H]FDDNP in absolute ethanol was > 98 % radiochemically pure as demonstrated by analytical HPLC radioflow chromatography (Fig. S3, Supplementary Material). [^{3}H]FDDNP was found to be stable in absolute ethanol medium stored in a freezer. The HPLC analysis of the stock solution of [^{3}H]FDDNP in ethanol at the end of the autoradiography work (10 weeks from the date of the procurement of [^{3}H]FDDNP) described herein showed a radiochemical purity of 94.4 % (Fig. 2).

[^{3}H]FDDNP in PBS/10 % EtOH solution was found to undergo autoradiolysis in time, which prompted us to conduct a kinetic analysis. Accordingly, two batches of [^{3}H]FDDNP in PBS/10 % ethanol were prepared and, at various time intervals up to 8 days, were analyzed in

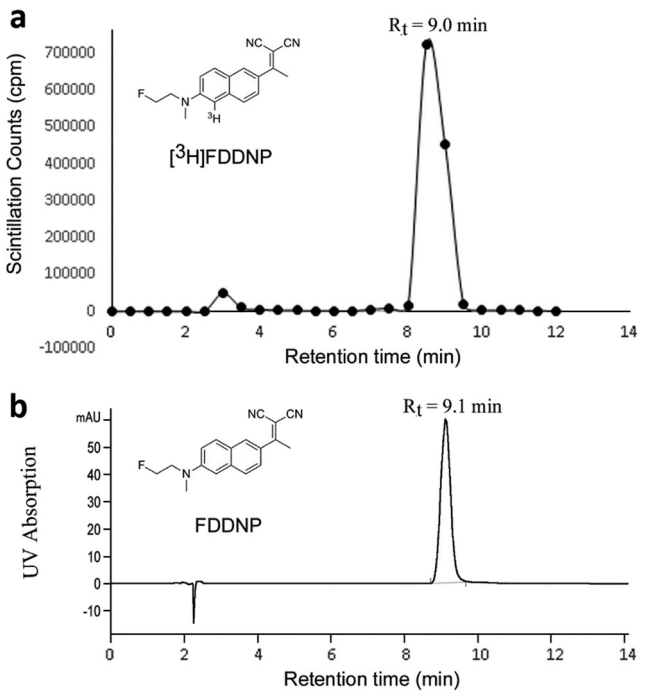

Fig. 2. The purity of the [^{3}H]FDDNP at the end of the autoradiography investigation as analyzed by analytical HPLC. Waters symmetry C18, 5 μm particle size, 4.6 × 150 mm column. Mobile phase: THF/MeOH/H_2O (2:1:2); flow rate: 0.5 ml/min. Detection: 0.5 min fractions counted by **a** scintillation for chromatogram; **b** 440 nm UV for chromatogram for an authentic sample of FDDNP.

duplicate by analytical HPLC. This analysis indicated that over time [^{3}H]FDDNP was gradually converted to [^{3}H]FENE and [^{3}H]H_2O, due to autoradiolysis. Under the analytical HPLC conditions, used [^{3}H]H_2O eluted, as expected, at the solvent front and [^{3}H]FENE was identified by injecting an authentic standard [16]. Interestingly, at the 8-day time point, only ~ 4 % of [^{3}H]FDDNP remained intact while [^{3}H]FENE was found to be the major product. The relevant data on the autoradiolysis of [^{3}H]FDDNP in PBS/10 % ethanol solution are summarized in the Supplementary Material, Table S1. Fig. 3 represents three possible autoradiolysis reactions: *ARR1*, *ARR2*, and *ARR3*.

Assuming that the autoradiolysis of [^{3}H]FDDNP in PBS/10 % EtOH mixture follows first-order kinetics, the above process can be described by a three compartmental model governed by the following set of first-order differential equations (1):

$$\begin{aligned}
\frac{d}{dt}C_{[^3\mathrm{H}]\mathrm{FDDNP}}(t) &= -(k_1+k_2)C_{[^3\mathrm{H}]\mathrm{FDDNP}}(t)\\
\frac{d}{dt}C_{[^3\mathrm{H}]\mathrm{FENE}}(t) &= k_1 C_{[^3\mathrm{H}]\mathrm{FDDNP}}(t) - k_3 C_{[^3\mathrm{H}]\mathrm{FENE}}(t)\\
\frac{d}{dt}C_{[^3\mathrm{H}]_2\mathrm{O}}(t) &= k_2 C_{[^3\mathrm{H}]\mathrm{FDDNP}}(t) + k_3 C_{[^3\mathrm{H}]\mathrm{FENE}}(t)
\end{aligned} \qquad (1)$$

where $C_{[^3\mathrm{H}]\mathrm{FDDNP}}(t)$, $C_{[^3\mathrm{H}]\mathrm{FENE}}(t)$, and $C_{[^3\mathrm{H}]_2\mathrm{O}}(t)$ represent the activity concentrations of [^{3}H]FDDNP, [^{3}H]FENE, and [^{3}H]H_2O, respectively at time t, and k_1, k_2, and k_3 are the rate constants (h^{-1}) for *ARR1*, *ARR2*, and *ARR3*, respectively (Fig. 3). As a result, Fig. 4 shows the best compartmental model curve fitting for the above kinetics.

The experimentally determined concentration of [^{3}H]FDDNP in PBS/10 % EtOH mixture was found to decrease steadily while that of [^{3}H]FENE increased with time. The concentrations of both [^{3}H]FDDNP and [^{3}H]FENE reached to about 50 % at ~ 50 h time point. Radioactivity concentration of [^{3}H]H_2O was found to increase gradually in a pseudo-linear manner even though both [^{3}H]FDDNP and [^{3}H]FENE could radiolyze to form [^{3}H]H_2O as predicted by the best model fit outlined in Fig. 4. At 201.5 h (*i.e.*, 8 days and 9.5 h), the kinetic model (Eq. 1) indicates the concentrations of [^{3}H]FDDNP, [^{3}H]FENE, and [^{3}H]H_2O to be about 2.5 to 5 %, 74 to 79 %, and 17 to 21 %, respectively, which compares well with the analytical HPLC data provided in Table S1 (Supplementary Material).

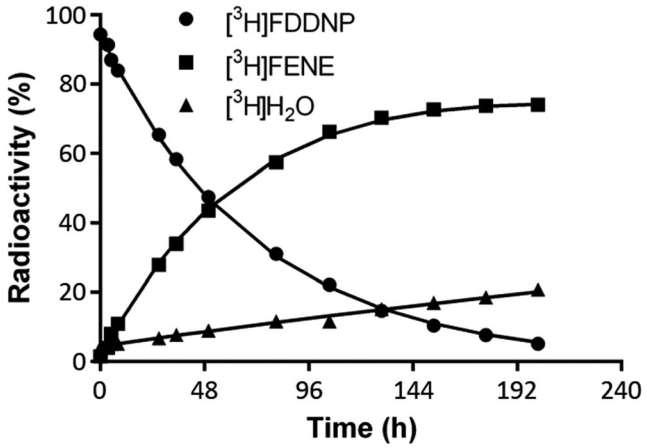

Fig. 4. The best model fit for the autoradiolysis of [^{3}H]FDDNP in PBS/10 % EtOH mixture to yield [^{3}H]FENE and [^{3}H]H_2O.

[^{3}H]FDDNP and [^{18}F]FDDNP Autoradiography Using the Thompson and Agdeppa Methods

Fig. 5 shows autoradiographs of Alzheimer's disease brain slices using methods from Thompson et al. [3] and Agdeppa et al. [6, 7] with [^{3}H]FDDNP and [^{18}F]FDDNP, respectively. The [^{3}H]FDDNP and [^{18}F]FDDNP images are not qualitatively different (Fig. 5b, d). The Thompson method (Fig. 5a, c) shows limited specific signal with significant non-specific signal in the white matter consistent with the previously reported results [3]. The Agdeppa method shows extensive plaque load and specific binding throughout the cortical gray matter (Fig. 5b, d).

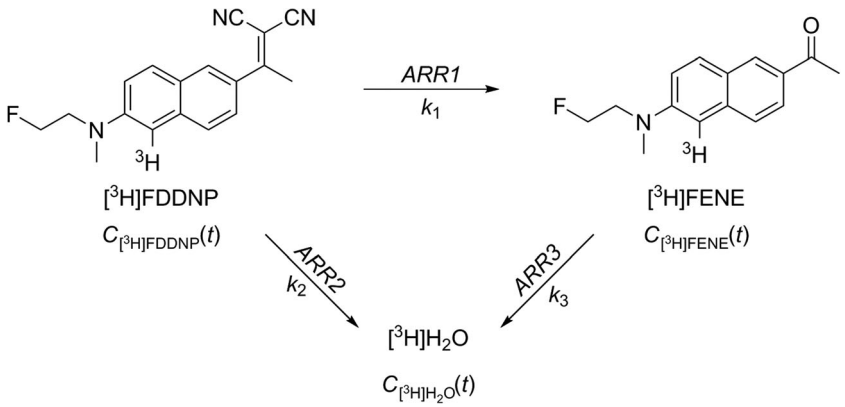

Fig. 3. Autoradiolysis reactions *ARR1*, *ARR2*, and *ARR3* of [^{3}H]FDDNP in PBS/10 % EtOH mixture.

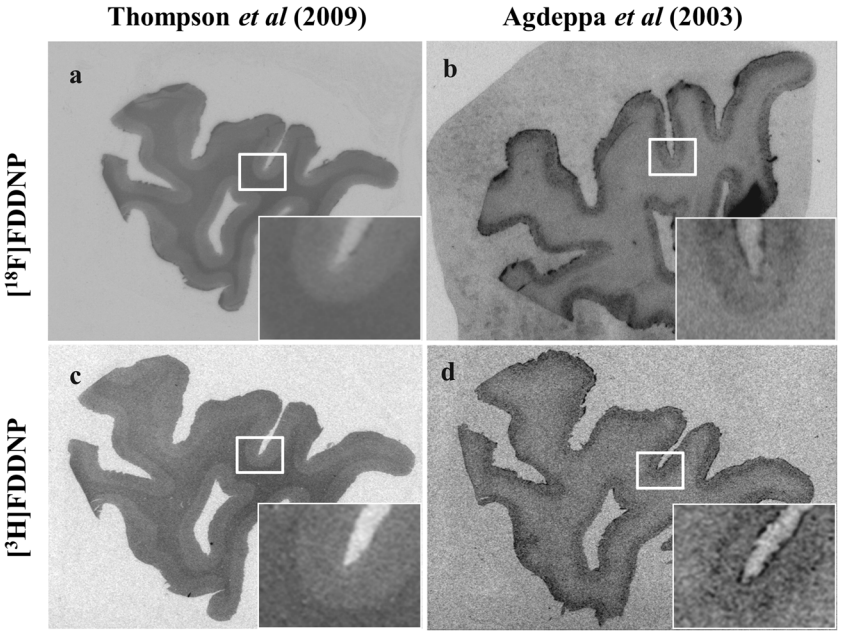

Fig. 5. **a** [^{18}F]FDDNP autoradiography using the method of Thompson et al. and **b** [^{18}F]FDDNP autoradiography using the method of Agdeppa et al. **c** [^{3}H]FDDNP autoradiography using the method of Thompson et al. and **d** [^{3}H]FDDNP autoradiography using the method of Agdeppa et al. Note the differential cortical binding to amyloid plaques between the two methods only due to the different experimental conditions of the autoradiography determinations. It could be surmised from Thompson et al. results that the high white matter labeling (**a**, **c**) may be an indication of presumptive radiolytic hydrolysis of the [^{3}H]FDDNP used, with resulting production of [^{3}H]FENE (Fig. 4). This is consistent with earlier observations from our laboratory that [^{18}F]FENE has preponderant high capacity, non-specific binding to white matter in the living human brain, presumably because of membrane intercalation (unpublished observations).

Micro-autoradiography

Fig. 6a shows a low magnification micro-autoradiograph of the medial temporal/hippocampal area of an AD brain performed using tau-pathology visualizing conditions. For orientation, this result is compared to Fig. 6b, reproduced from Ref. [17].

The Aβ protein aggregates (Fig. 6c) are clearly visible, albeit overexposed under these conditions. The autoradiography signal compares to the anti-Aβ immunohistochemistry labeling (Fig. 6d). Tau-positive cells are also visible (Fig. 6e) and compared to the anti-tau immunohistochemistry (Fig. 6f).

Discussion

This work outlines why rigorous *in vitro* work is crucial to ascertain accurate translation of these results to *in vivo* settings, which involves synthetic considerations, radiochemical stability of the tracer, and possible autoradiolysis and autoradiographic protocol validation considerations for accurate interpretation of results. The experimental methods presented in this work focus on (1) demonstrating specific FDDNP binding to Aβ and tau neuroaggregates in brain slices of Alzheimer's disease patients using high-resolution micro-autoradiography and (2) comparing these results with those reported earlier by Thompson et al. [3]. Accordingly, we have (1) synthesized and used pure [^{18}F]FDDNP [16] and pure [^{3}H]FDDNP for these experiments, (2) compared the effect of solvents (*e.g.*, EtOH) used in the primary incubations, and (3) compared variation in differentiation conditions.

Organic Synthesis

Tritium labeling is most commonly achieved through catalytic reduction with tritium gas, reduction with [^{3}H] sodium borohydride or [^{3}H] lithium aluminum hydride, methylation with [^{3}H] methyl iodide, or a carbanion quench with tritiated water [18]. For the preparation of the tritium-labeled analog of FDDNP, we selected to exchange halogen for tritium at the aromatic ring by palladium catalyzed hydrogenolysis by using [^{3}H]H_2.

The precursors for the tritium labeling were prepared according to Scheme S1 (Supplemental Material). Chemoselective bromination of starting naphthalene derivative **1** gave single product **2**, which was fluorinated with diethylaminosulfur trifluoride (DAST) to compound **3**. The position of bromine at the aromatic ring in **3** was unambiguously established by 1D and 2D NMR spectroscopy (Supplemental Material). Knoevenagel reaction of ketone **3** with malononitrile in pyridine furnished brominated FDDNP derivative **4**. As indicated in Scheme S1

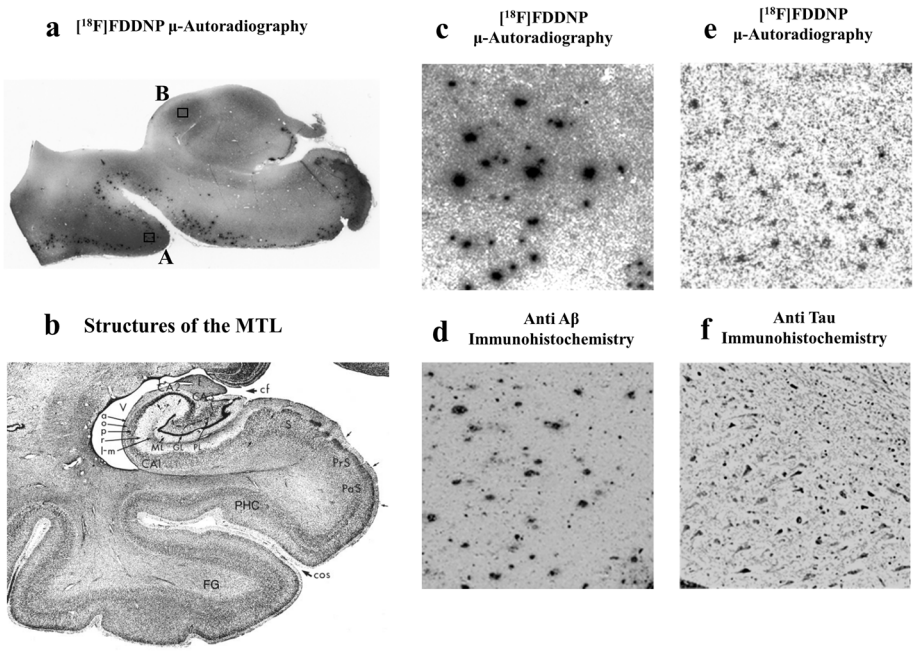

Fig. 6. **a** Micro-autoradiography using the method of Agdeppa et al. shows both Aβ and tau neuropathology in the hippocampus. Pullouts show **c** Aβ (inset box A) autoradiography and **d** IHC and **e** tau (inset box B) autoradiography and **f** IHC. Aβ autoradiography was thresholded to reduce background; tau autoradiography was filtered using difference of Gaussian edge finding. **b** The structures of the MTL image is reproduced from Ref. [17].

(Supplementary Material), both the bromo analogs **3** and **4** are potentially the synthetic precursors for the preparation of the target [^{3}H]FDDNP. Despite the fact that introduction of a radiolabel in radiosynthesis is generally preferred to be accomplished in the final step of the reaction sequences, an independent experimental work discussed above revealed that hydrogenolysis of **3** with [^{1}H]H_2/Pd/C into [^{3}H]FENE, followed by Knoevenagel reaction in the last step (*Path b*), is in this case superior to *Path a* (Schemes S2 and S3, Supplementary Material). The crude product [^{3}H]FDDNP was purified by semi-preparative HPLC to obtain > 98 % radiochemically pure [^{3}H]FDDNP with a specific activity of 20.2 Ci/mmol. To mitigate autoradiolysis, the product was dissolved in absolute ethanol and stored in a freezer.

Autoradiolysis of [^{3}H]FDDNP

The propensity for autoradiolysis of tritium-labeled tracers is a well-known phenomenon [15, 18–20]. Autoradiolysis is most significant with tritiated analogs because the low energy of β^- emission (mean decay energy for tritium is 5.7 keV) is almost entirely dissipated within the compound itself (mean path length for β^- particle emission from tritium in water is 0.47 μm). Since the average energy of carbon–carbon bonds in organic compounds is only about 5–10 eV, the 5.7 KeV decay energy of tritium (which is absorbed very efficiently by the tracer itself) can cause decomposition of large number of the tracer molecules [15]. Hence, the control of autoradiolysis of tritium-labeled compounds is much more difficult than for compounds labeled with other radioisotopes which generally have much higher decay energies (>> 5.7 keV) and longer mean path lengths (> 40 μm in water) for the particle emissions [15]. The autoradiolysis of tritiated compounds has consequently been studied in rather more detail than that of other radiolabeled products. Several factors such as the specific activity of the tracer and the inherent stability of the compound and storage solvent can all play a role in the autoradiolysis of tritium-labeled compounds. In many cases, aqueous solvents or even the presence of residual water in organic solvents have been shown to exacerbate the autoradiolysis of tritiated analogs [20]. Thus, it is imperative the tritium-labeled derivatives are stored in appropriate solvents (*e.g.*, absolute ethanol) at low temperatures to minimize autoradiolysis. Importantly, the radiochemical purity of the tritiated compounds always needs to be verified just prior to *in vitro* utilization.

Tritium-labeled FDDNP in absolute ethanol at − 20 °C was found to undergo autoradiolysis only by about 1.8 % per month. But [^{3}H]FDDNP in PBS/10 % ethanol was rapidly converted to [^{3}H]FENE and [^{3}H]H_2O due to autoradiolysis (Table S1, Supplementary Material). Formation of [^{3}H]H_2O due to proton/tritium exchange in tritiated derivatives has been well described in the literature [12, 17] and likely plays a similar role with [^{3}H]FDDNP in PBS/10 % ethanol. The mechanism of autoradiolytic formation of [^{3}H]FENE was not investigated in this study. However, base catalyzed hydrolysis of FDDNP is known to produce FENE [16]. Interestingly, at the 201.5 h (~ 8.5 days) time-point,

only 4 % of [^{3}H]FDDNP remained intact while [^{3}H]FENE was found to be the major product (Table S1, Supplementary Material) when the tracer was stored in PBS/10 % ethanol. This observation clearly demonstrates the importance of determining the radiochemical purity of [^{3}H]FDDNP at the time of *in vitro* experiments. Considering the extreme sensitivity of [^{3}H]FDDNP in PBS/10 % ethanol to autoradiolysis, its radiochemical purity was ascertained to be 95–98 % by analytical HPLC at the time of all the *in vitro* experiments of this investigation. Thompson et al. [3] described that [^{3}H]FDDNP (13 Ci/mmol) was obtained as custom syntheses by an undisclosed synthesis method from GE Healthcare Life Sciences (Little Chalfont, UK), but unfortunately neither evidence of the radiochemical purity of [^{3}H]FDDNP nor stability data, either upon receipt or at the time of the *in vitro* study, were provided. Therefore, considering the inherent instability of [^{3}H]FDDNP, as reported in this work, legitimate concerns over the validity of their *in vitro* data and the conclusions drawn based on them would exist.

Construct Validity of the Autoradiography Experiments

In order to contextualize the results of these *in vitro* experiments, several assumptions underlying the autoradiography technique must be considered.

First, *in vitro* autoradiography assumes that the radiolabeled tracer is pure at the outset and maintains its chemical purity throughout the binding experiment. As discussed, Fig. 4 demonstrates that [^{3}H]FDDNP rapidly undergoes autoradiolysis to [^{3}H]FENE and [^{3}H]H_2O when left in PBS/10 % EtOH. Autoradiolysis of [^{3}H]FDDNP in aqueous media such as PBS/10 % EtOH is significant even in short period of times (Table S1, Supplementary Material). Thus, if [^{3}H]FDDNP is stored in an aqueous solution or the solution is not prepared immediately prior to use from a 100 % EtOH stock solution, the integrity of the primary incubation and differentiation steps will be of serious concern. Hence, it is critically necessary to begin with very high purity [^{3}H]FDDNP (or [^{18}F]FDDNP) and to store it appropriately in absolute EtOH until just before use. This issue cannot be ignored. FDDNP decomposes into FENE which has very different binding constants against protein aggregates than FDDNP, and also binds substantially to brain white matter structures [6]. We have previously shown that [^{3}H]FENE radiolabeling of the intended neuroaggregates is not optimal [6].

Second, *in vitro* autoradiography assumes that the primary incubation—*e.g.*, presence or absence of EtOH, or the pH of the buffer—creates a comparable environment for probe binding to the environment *in vivo*. Thompson et al. used 10 % EtOH during primary incubation for all the tracers tested [3]. Such experimental conditions implicitly assume that the EtOH concentration does not affect the binding properties of the imaging probe. However, Agdeppa et al. disclosed earlier experimental methods using less than 1 % EtOH in PBS to optimally bind FDDNP to target proteins *in vitro* and, under *in vivo* conditions, given the low injected mass dose of the radiotracer, is the nanomolar high affinity binding the driver for the signal [6, 7]. Higher concentrations of EtOH will produce conditions that disrupt FDDNP binding *in vitro* and are not indicative of the binding characteristics observed *in vivo*. The fact that high concentrations of organic solvents in the primary incubation affect the binding affinity of DDNP derivatives is well documented [6, 7]. Amyloid and tau aggregates have a hydrophobic binding domain, and FDDNP binding, like other 2,6-disubstituted naphthalene derivatives, is strongly dependent on the dipole moment of the molecule [21, 22], which makes the molecule highly sensitive to solvent polarity. Therefore, solvent conditions used for binding determinations in the primary incubation solution play a critical role and affects the specific binding of the probe.

Finally, the three compounds tested comparatively by Thompson et al. [3], the "tritiated" analog of FDDNP, the tritiated derivative of PIB, and the ^{14}C-labeled derivative of SB-13, have unique binding sites on amyloid aggregates [6, 7, 23, 24]. It is therefore imprudent to assume that these compounds will readily bind to amyloid aggregates under identical *in vitro* conditions. Logically, instead, both the primary incubation and the differentiation step must be tested and optimized for each tracer.

Fig. 5 demonstrates the effect of increasing concentration of EtOH on FDDNP binding to amyloid aggregates. Fig. 5a and c shows very little FDDNP specific binding using PBS/10 % EtOH for both primary incubation and differentiation (Thompson et al. conditions [3]). Fig. 5b and d, by contrast, shows significant specific binding to amyloid aggregates in cortical gray matter using <1 % EtOH in the primary incubation (Agdeppa et al. conditions [6, 7]). Fig. 5 demonstrates that primary incubation with 10 % EtOH interferes with FDDNP binding to amyloid aggregates, and thus little specific signal is observed. In parallel, weak differentiation using the same 10 % EtOH solution fails to appreciably differentiate the specific from the non-specific signal making the background signal in the white matter more visible after washing. These high EtOH concentrations in the primary incubation solvent invalidate the results, even before taking into account that the questionable purity of the [^{3}H]FDDNP used may also degrade the results. Fig. 6c and d, using [^{18}F]FDDNP micro-autoradiography with temporal lobe brain slices of an AD subject, demonstrate labeling of amyloid aggregates (Fig. 6c) as confirmed with Aβ immunohistochemistry in an adjacent tissue slice (Fig. 6d). Similarly, Fig. 6e shows [^{18}F]FDDNP-labeled tau-tangles in the pyramidal neurons of the hippocampus in comparison with tau immunohistochemistry in an adjacent slice.

Figs. 5 and 6 show that FDDNP clearly binds to its target proteins under these *in vitro* conditions. Thus, the assumption of Thompson et al. [3] that a negative *in vitro* experiment under a particular set of experimental conditions

demonstrated that the probe did not bind to the same target tissues *in vivo* was invalid. Amyloid/tau binding, though it entices the use of *in vivo* receptor binding models and Logan graphical analysis, is significantly different from classical receptor binding [25–28]. The dynamic nature of amyloid/tau aggregates, their heterogeneous constitution as well as their multiple binding sites, and non-membrane localization, all work against purely receptor–ligand binding assumptions. Again, all of these without taking into consideration the undocumented purity of the [^{3}H]FDDNP used in their experiments [3], which in itself calls into question any conclusions,

Finally, for *in vivo* use of PET probes, *in vitro* conditions should be always optimized to demonstrate the sensitivity and specificity to a given tissue target (*e.g.*, amyloid or tau aggregates). Thus, when it comes to selecting, qualifying, and validating new tracers as molecular imaging probe candidates, it is crucial to develop and use *postmortem* autoradiography methods that are rigorous, well validated, and with thorough investigation of the impact of binding conditions *versus* actual tissue targets. Most often these experiments are not designed to assess unknown off-target binding, and may be inadvertently designed to deactivate such competitive processes like active enzymes that are otherwise present under *in vivo* conditions. The previously unrecognized *in vitro* binding of the purported tau specific agent AV-1451 to MAO A and MAO B [29] offers a clear example of this issue. This previously unknown off-target binding was only recently discovered when *in vivo* results could not be explained based upon tau-binding (the purported specific target of the agent) [30–33]. A CNS panel evaluation with 50 plus proteins to gauge any possible off-target activity, prior to further characterization and/or development of the probe, would likely have negated the use of AV-1451 (and THK-5351) as viable clinical PET ligands before any autoradiograms or *in vivo* animal or human studies had ever been carried out.

Thompson et al. [3] and other publications from the same laboratory [4, 5] serve as excellent examples of why *in vitro* results must be used with great care to explain *in vivo* phenomena or to simulate *in vivo* conditions. This is not new; early concepts underlying these issues were established more than two decades ago during the development of the PET methodology [34]. *In vitro* conditions have to be as close to the physiological conditions as possible to ensure that the targeted protein maintains its physiological *in vivo* conformation to guarantee that both the active sites of the targeted protein and the radioligand are solvated nearly in the same way as under physiological conditions. This is the only way *in vitro* binding affinity estimates will have any relevance for the interpretation of *in vivo* PET binding. The present work also adds some specifics to the tissue targeting of neuroaggregates and serves to critically examine the assumptions involved in these types of *in vitro* characterizations, which should have been avoided based on the acquired experience of PET probe development [35].

Understanding the *in vivo* specificity of the tracer is essential in order to interpret *in vivo* imaging results. *In vitro* experiments, such as those described in this work, are an important first step, taking inclusive into consideration the caveats that characterize specificity in rigorous terms (*e.g.*, thioflavin and Congo Red are not specific for a given proteinopathy). However, the mere correlation of one set of results (*e.g.*, *in vitro* data) with another (*e.g.*, *in vivo* data) does not imply a direct causative relationship. Indeed, the literature is replete with examples of correlations for which causation is nothing more than an incidental coincidence [36–39].

Conclusions

The evidence from this work indicates that the integrity of the experiments described by Thompson et al. [3] were compromised, invalidating their *in vitro* conclusions, which openly ignores available *in vitro* data in humans, including neuropathological fluorescence, autoradiographic and Scatchard plot analysis [40], as well as PET scan results in living subjects with a variety of neurodegenerative diseases. Since [^{3}H]FDDNP is highly susceptible to autoradiolysis and suffers rapid decomposition, the chemical and radiochemical integrity of the [^{3}H]FDDNP at the time of the *in vitro* binding experiments is an essential piece of information to ascertain validity of their results. Besides, the use of 10 % EtOH solution as primary incubation solution for [^{3}H]FDDNP binding determinations seems to be a compounding fatal cause of the poor autoradiography results reported with [^{3}H]FDDNP. These confirm well-established evidence on the limitations of *in vitro* binding results portrayed as irrefutable predictors of *in vivo* binding of molecular imaging probes. These are also reminders that observations from poorly executed experiments would unavoidably lead to wrong interpretations that can be perpetuated and even later reproduced or assumed without further analysis.

Acknowledgments. Special thanks to the excellent reviewers and the editor (RG) for constructive comments and valuable advice, which have been incorporated into the manuscript. This work was supported by grants from the Slovenian Research Agency (Research Core Funding Grant P1-0230 and project J1-8147) and by grants P01-AG025831, AG13308, P50 AG 16570, MH/AG58156, MH52453, and AG10123 from the National Institutes of Health; contract DE-FC03-87-ER60615 from the Department of Energy. J.R.B. gratefully acknowledges the Elizabeth and Thomas Plott Endowment in Gerontology. This work was also partially supported within the infrastructures of the EN-FIST Centre of Excellence, Trg Osvobodilne fronte 13, 1000 Ljubljana, Slovenia, and the Centre for Research Infrastructure at the Faculty of Chemistry and Chemical Technology of the University of Ljubljana. The NMR analysis at UCLA Department of Chemistry was supported by the National Science Foundation equipment grant no. CHE-1048804.

Compliance with Ethical Standards

Conflict of Interest

The University of California, Los Angeles, owns a U.S. patent (6,274,119) entitled "Methods for Labeling β-Amyloid Plaques and Neurofibrillary Tangles," which has been licensed to TauMark, LLC. N.S., G.W.S., S.-C.H., A.P., and J.R.B. are among the inventors. N.S., S.-C.H., G.W.S., and J.R.B. have equity interest in TauMark, LLC. All other authors report no financial conflicts of interest.

References

1. Chronback LJ, Meehl PE (1955) Construct validity in psychological tests. Psychol Bull 52:281–302
2. Cole GB, Keum G, Liu J, Small GW, Satyamurthy N, Kepe V, Barrio JR (2010) Specific estrogen sulfotransferase (SULT1E1) substrates and molecular imaging probe candidates. Proc Natl Acad Sci U S A 107:6222–6227
3. Thompson PW, Ye L, Morgenstern JL, Sue L, Beach TG, Judd DJ, Shipley NJ, Libri V, Lockhart A (2009) Interaction of the amyloid imaging tracer FDDNP with hallmark Alzheimer's disease pathologies. J Neurochem 109:623–630
4. Lockhart A, Lamb JR, Osredkar T et al (2007) PIB is a non-specific imaging marker of amyloid-beta (Aβ) peptide-related cerebral amyloidosis. Brain 1(30):2607–2615
5. Ye L, Morgenstern JL, Gee AD, Hong G, Brown J, Lockhart A (2005) Delineation of positron emission tomography imaging agent binding sites on β-amyloid peptide fibrils. J Biol Chem 280:23599–23604
6. Agdeppa ED, Kepe V, Liu J, Flores-Torres S, Satyamurthy N, Petric A, Cole GM, Small GW, Huang SC, Barrio JR (2001) Binding characteristics of radiofluorinated 6-dialkylamino-2-naphthylethylidene derivatives as positron emission tomography imaging probes for β-amyloid plaques in Alzheimer's disease. J Neurosci 21:RC189
7. Agdeppa ED, Kepe V, Petric A et al (2003) In vivo detection of (*S*)-naproxen and ibuprofen binding to plaques in the Alzheimer's brain using the positron emission tomography molecular imaging probe 2-(1-{6-[(2-[^{18}F]fluoroethyl)(methyl)amino]-2-naphthyl}ethylidene)malononitrile. Neuroscience 117:723–730
8. Bancroft JD, Stevens A (eds) (1990) Theory and practice of histological techniques, 3rd edn. Churchill Livingstone, Edinburgh
9. Small GW, Kepe V, Ercoli LM, Siddarth P, Bookheimer SY, Miller KJ, Lavretsky H, Burggren AC, Cole GM, Vinters HV, Thompson PM, Huang SC, Satyamurthy N, Phelps ME, Barrio JR (2006) PET of brain amyloid and tau in mild cognitive impairment. N Engl J Med 355:2652–2663
10. Kepe V, Bordelon Y, Boxer A, Huang SC, Liu J, Thiede FC, Mazziotta JC, Mendez MF, Donoghue N, Small GW, Barrio JR (2013) PET imaging of neuropathology in tauopathies: progressive supranuclear palsy. J Alzheimers Dis 36:145–153
11. Smid LM, Kepe V, Vinters HV, Bresjanac M, Toyokuni T, Satyamurthy N, Wong KP, Huang SC, Silverman DH, Miller K, Small GW, Barrio JR (2013) Postmortem 3-D brain hemisphere cortical tau and amyloid-β pathology mapping and quantification as a validation method of neuropathology imaging. J Alzheimers Dis 36:261–274
12. Barrio JR, Small GW, Wong KP, Huang SC, Liu J, Merrill DA, Giza CC, Fitzsimmons RP, Omalu B, Bailes J, Kepe V (2015) In vivo characterization of chronic traumatic encephalopathy (CTE) using [F-18]FDDNP-PET brain imaging. Proc Natl Acad Sci USA 112:E2039–E2047
13. Klunk WE, Engler H, Nordberg A, Wang Y, Blomqvist G, Holt DP, Bergström M, Savitcheva I, Huang GF, Estrada S, Ausén B, Debnath ML, Barletta J, Price JC, Sandell J, Lopresti BJ, Wall A, Koivisto P, Antoni G, Mathis CA, Långström B (2004) Imaging brain amyloid in Alzheimer's disease with Pittsburgh compound-B. Ann Neurol 55:306–319
14. Verhoeff NPLG, Wilson AA, Takeshita S, Trop L, Hussey D, Singh K, Kung HF, Kung MP, Houle S (2004) In-vivo imaging of Alzheimer's disease β-amyloid with [11C]SB-13 PET. Am J Geriatr Psychiatry 12:584–595
15. Bayly RJ, Evans EA (1966) Stability and storage of compounds labelled with radioisotopes. J Label Compd 2:1–34
16. Liu J, Kepe V, Žabjek A, Petrič A, Padgett HC, Satyamurthy N, Barrio JR (2007) High-yield, automated radiosynthesis of 2-(1-{6-[(2-[^{18}F]fluoroethyl)(methyl)amino]-2-naphthyl}ethylidene)malononitrile ([^{18}F]FDDNP) ready for animal or human administration. Mol Imaging Biol 9:6–16
17. Amaral DG (1999) Introduction: what is where in the medial temporal lobe? Hippocampus 9:1–6
18. Voges R, Heys JR, Moenius T (2009) Preparation of compounds labeled with tritium and Carbon-14. Wiley, Chichester
19. Tkachenko SE, Karpov NA, Fedoseev VM (2000) Autoradiolysis of labeled organic compounds. Radiochemistry 42:211–227
20. Waterfield WR, Spanner JA, Stanford FG (1968) Tritium exchange from compounds in dilute aqueous solutions. Nature 218:472–473
21. Jacobson A, Petrič A, Hogenkamp D et al (1996) 1,1-Dicyano-2-[6-(dimethylamino)naphthalene-2-yl]propene (DDNP): a solvent polarity and viscosity sensitive fluorophore for fluorescence microscopy. J Am Chem Soc 118:5572–5579
22. Petric A, Johnson SA, Pham HV, Li Y, Ceh S, Golobic A, Agdeppa ED, Timbol G, Liu J, Keum G, Satyamurthy N, Kepe V, Houk KN, Barrio JR (2012) Dicyanovinylnaphthalenes for neuroimaging of amyloids and relationships of electronic structures and geometries to binding affinities. Proc Natl Acad Sci U S A 109:16492–16497
23. Kung MP, Hou C, Zhuang ZP, Skovronsky D, Kung HF (2004) Binding of two potential imaging agents targeting amyloid plaques in postmortem brain tissues of patients with Alzheimer's disease. Brain Res 1025:98–105
24. Price JC, Klunk WE, Lopresti BJ, Lu X, Hoge JA, Ziolko SK, Holt DP, Meltzer CC, DeKosky ST, Mathis CA (2005) Kinetic modeling of amyloid binding in humans using PET imaging and Pittsburgh compound-B. J Cereb Blood Flow Metab 25:1528–1547
25. Logan J, Fowler JS, Volkow ND, Wang GJ, Ding YS, Alexoff DL (1996) Distribution volume ratios without blood sampling from graphical analysis of PET data. J Cereb Blood Flow Metab 16:834–840
26. Logan J (2000) Graphical analysis of PET data applied to reversible and irreversible tracers. Nucl Med Biol 27:661–670
27. Shogi-Jadid K, Barrio JR, Kepe V et al (2005) Imaging β-amyloid fibrils in Alzheimer's disease: a critical analysis through simulation of amyloid fibril polymerization. Nucl Med Biol 32:337–351
28. Shogi-Jadid K, Barrio JR, Kepe V et al (2006) Exploring a mathematical model for the kinetics of β-amyloid molecular imaging probes through a critical analysis of plaque pathology. Mol Imaging Biol 8:151–162
29. Xia CF, Arteaga J, Chen G, Gangadharmath U, Gomez LF, Kasi D, Lam C, Liang Q, Liu C, Mocharla VP, Mu F, Sinha A, Su H, Szardenings AK, Walsh JC, Wang E, Yu C, Zhang W, Zhao T, Kolb HC (2013) [^{18}F]T807, a novel tau positron emission tomography imaging agent for Alzheimer's disease. Alzheimers Dement 9:666–676
30. Vermeiren C, Mercier J, Viot D, Mairet-Coello G, Hannestad J, Courade JP, Citron M, Gillard M (2015) T807, a reported selective tau tracer, binds with nanomolar affinity to monoamine oxidase a. Alzheimer's Dement Suppl 11:P283
31. Mitsis EM, Riggio S, Kostakoglu L, Dickstein DL, Machac J, Delman B, Goldstein M, Jennings D, D'Antonio E, Martin J, Naidich TP, Aloysi A, Fernandez C, Seibyl J, DeKosky ST, Elder GA, Marek K, Gordon W, Hof PR, Sano M, Gandy S (2014) Tauopathy PET and amyloid PET in the diagnosis of chronic traumatic encephalopathies: studies of a retired NFL player and of a man with FTD and a severe head injury. Transl Psychiatry 4:e441
32. Gandy S, DeKosky ST (2014) [^{18}F]-T807 tauopathy PET imaging in chronic traumatic encephalopathy. F1000 Res 3:229
33. Barrio JR (2018) The irony of PET tau probe specificity. J Nucl Med 59:115–116
34. Frey KA, Albin RL (1997) Neuroanatomical methods receptor binding techniques. Current protocols in neuroscience. Wiley, New York, pp 1.4.1–1.4.14
35. Barrio JR (2004) The molecular basis of disease. In: Phelps ME (ed) PET—molecular imaging and its biological applications. Springer, New York, pp 270–320
36. Hallberg O, Johansson O (2009) Sleep on the right side—get cancer on the left? Pathophysiology 17:157–160
37. Hallberg O, Johansson O (2002) Cancer trends during the 20th century. ACNEM 21:1–6
38. Quinn GE, Shin CH, Maguire MG, Stone RA (1999) Myopia and ambient lighting at night. Nature 399:113–114
39. Wakefield AJ, Murch SH, Anthony A et al (1998) Ileal-lymphoid-nodular hyperplasia, non-specific colitis, and pervasive developmental disorder in children. Lancet 351:637–641 Retracted in 2010
40. Agdeppa ED, Kepe V, Shoghi-Jadid K et al (2003) 2-Dialkylamino-6-acylmalononitrile substituted naphthalenes (DDNP analogs): novel diagnostic and therapeutic tools in Alzheimer's disease. Mol Imaging Biol 5:407–417